Revista Mexicana de Astronomía y Astrofísica, **60**, 205–216 (2024)

https://doi.org/10.22201/ia.01851101p.2024.60.02.01

LIGHT AND FREQUENCY ANALYSIS OF DETACHED ECCENTRIC BINARY SYSTEM DT CAM WITH PRE-MAIN SEQUENCE COMPONENT

Tuncay Özdemir[1] and Birol Gürol[2]

Received September 3 2023; accepted February 27 2024

ABSTRACT

In this study we analyzed *TESS* data of detached eccentric binary system DT Cam and we obtained the first physical parameters of the components. We found that the out-of-eclipse variation of the system shows a small amplitude periodic feature. Most of the frequencies obtained are related with the orbital variation except one, for which the period was determined as ≈0.605 days. The masses and radii of the primary and secondary components were calculated as $M_1 = 1.793 M_\odot$, $M_2 = 1.414 M_\odot$, $R_1 = 1.355 R_\odot$, and $R_2 = 1.522 R_\odot$, respectively. Considering the physical properties of the primary component we concluded that it is a rotational variable. We found that the massive component is smaller than the low-mass component. It seems that the secondary component is a pre-main sequence star, which is important for the understanding of stellar structure and evolution.

RESUMEN

Se analizan datos de *TESS* sobre la binaria excéntrica DT Cam y se obtienen por primera vez los parámetros físicos de las componentes. Encontramos una variación periódica de pequeña amplitud fuera de eclipse. Muchas de las frecuencias obtenidas se relacionan con la variación orbital, excepto una, cuyo período se determinó como ≈0.605 días. Se calculan las masas y radios de las componentes primaria y secundaria, y se obtienen como resultados $M_1 = 1.793 M_\odot$, $M_2 = 1.414 M_\odot$, $R_1 = 1.355 R_\odot$, y $R_2 = 1.522 R_\odot$. Dadas las propiedades físicas de la primaria concluimos que es un variable rotacional. Encontramos que la componente masiva es más pequeña que la compañera de baja masa. Al parecer, la secundaria es una estrella pre-secuencia principal, lo cual es importante para entender la estructura y evolución estelares.

Key Words: binaries: eclipsing — stars: fundamental parameters — stars: individual: DT Cam — stars: rotation — techniques: photometric

1. INTRODUCTION

DT Cam (TIC 87251422, HD 33500, $\alpha_{2000} = 05^h13^m57^s.69$, $\delta_{2000} = +56^\circ\,30'\,28''.61$, $V = 8^m.13$) is classified as a spectroscopic binary in the Simbad[3] database. The spectral type and distance of the system are given as A2 (Cannon and Pickering 1993) and 184 pc (*Gaia* Collaboration 2022), respectively. The system is defined as an Algol-type eclipsing binary by Otero et al. (2005) with an orbital period of P=14.132500 days, and it is included in the GCVS catalogue[4].

In the catalogue published by McDonald et al. (2012), the system's distance (d), effective temperature ($T_{\rm eff}$), and luminosity (L) are given as $d = 255.750$ pc, $T_{\rm eff} = 7948$ K, and $L = 27.52 L_\odot$, respectively. In the Eclipsing Binary Catalogue published by Avvakumova et al. (2013) the system is classified as DM (detached main sequence system) with depth of the primary minima as $0^m.06$ which is probably mistyped. By analyzing the eclipse timing diagram of the system, Kim et al. (2018) found the orbital period and the phase of the secondary minima as $P = 7.0662668$ days and 0.578, respectively.

[1]Department of Physics, Faculty of Arts and Sciences, İnönü University, Malatya, Turkey.
[2]Department of Astronomy and Space Sciences, Ankara University Science Faculty, Tandoğan, Ankara, Turkey.
[3]https://simbad.cds.unistra.fr/simbad/.
[4]http://www.sai.msu.su/gcvs/cgi-bin/search.html.

TABLE 1

PARAMETERS OF THE LIGHT CURVE AND THE $(O-C)$ ANALYSES OF DT CAM*

Parameter	Value
i(deg)	87.69 (0.19)
T_1(K)	8800
T_2(K)	7382 (75)
L_1(%)	66.4 (0.7)
L_2(%)	33.6 (0.6)
L_3(%)	0.0
R_1/a	0.068(3)
R_2/a	0.064(2)
e	0.188(0.010)
$\omega(deg)$	49.2(1.3)
U(yr)	>100

*Obtained by Zasche et al.(2018).

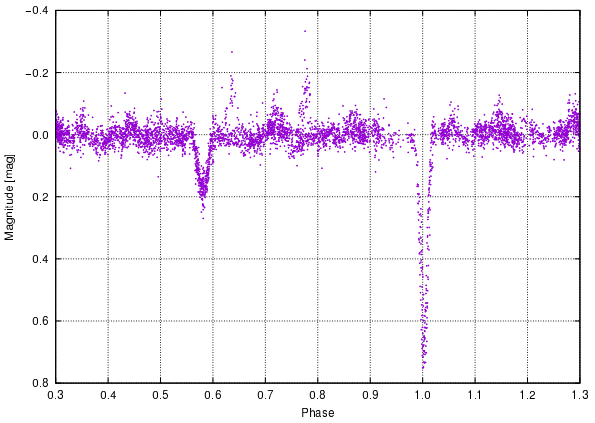

Fig. 1. Unfiltered light curve of ASCC 178636 (DT Cam) observed from MASCARA published by Burggraaff et al. (2018). The color figure can be viewed online.

Zasche et al. (2018) obtained the first light curve and $(O-C)$, and analysed the system by using unfiltered and special SuperWASP observations; their system parameters are given in Table 1.

By using Gaia DR2 data, Kervella et al. (2019) obtained the color excess, system's radial velocity, mass and radius of the primary component as $E(B-V) = 0.087$, $V_R = 33.881\,\mathrm{km/s}$, $M_1 = 2.2M_\odot$ and $R_1 = 1.862R_\odot$, respectively. Later, using Gaia EDR3 data, Kervella et al. (2022) updated some of the parameters as $V_R = 33.76\,\mathrm{km/s}$, $M_1 = 2.20M_\odot$ and $R_1 = 1.85R_\odot$. In the catalogue of EA-type eclipsing binaries observed by *TESS* and published by Shi et al. (2022) the system's orbital period was given as 14.1325 days. Based on the Multi-site All-Sky CAmeRA (MASCARA) observations (see Figure 1) published by Burggraaff et al. (2018) the depth of the primary and secondary minima were given as $0^m.75$ and $0^m.2$, respectively. In Figure 1, although scattering is observed at maximum light, there are also traces of a periodic variation which can be related to pulsation in the system.

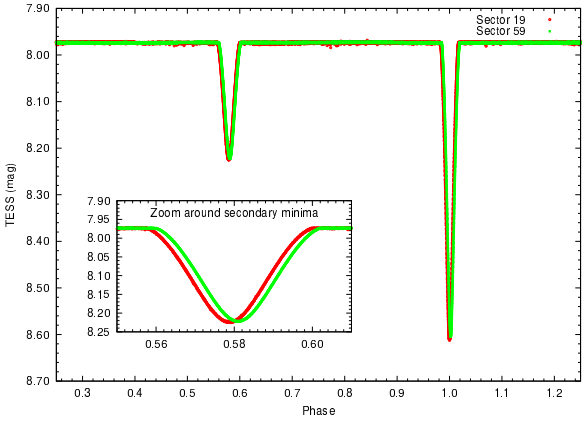

Fig. 2. The light curve of DT Cam (TIC 87251422) obtained from MAST archive for Sectors 19 (red) and 59 (green). The orbital phase is calculated by using equation (1). The color figure can be viewed online.

2. THE *TESS* DATA AND LIGHT ELEMENTS

The observations of DT Cam were made by the Transiting Exoplanet Survey Satellite (*TESS*) (Ricker et al. 2015) in Sectors 19 and 59 with each sector having ≈27.4 days of observations with nearly 2 min (SC: Short Cadence) exposure time. The *TESS* data are available in the MAST (Barbara A. Mikulski Archive for Space Telescopes[5]) archive. In this study we prefer to use the raw SAP (simple aperture photometry) data. A total of 35,860 observations of the system were obtained and the time span is nearly 1120.6 days. The light elements of the system are given in the *TESS* Eclipsing Binary Catalogue[6] published by Prša et al. (2022) as,

$$Min.I(BJD) = 2458825.166288(0.000014) + 7.0661708(0.000206) \times E\,. \quad (1)$$

In Figure 2 we plot the light curve of the system obtained in Sectors 19 and 59 by using the light elements given by Prša et al. (2022). As can be seen in the zoomed inner plot the secondary minima for both sectors do not overlap with each other which indicates that the light elements of the system need

[5] https://mast.stsci.edu/portal/Mashup/Clients/Mast/Portal.html.

[6] http://tessebs.villanova.edu/.

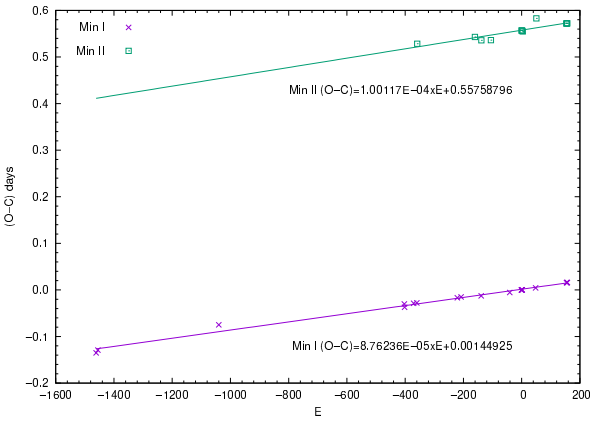

Fig. 3. $(O-C)$ variation and linear fit obtained for DT Cam by using equation (1) of Prša et al. (2022). The color figure can be viewed online.

to be refined. The same situation occurs for the primary minima too but it is not shown here. Additionally from the light curve we can say that the eclipsing system is composed of two spherical components in detached (D) configuration, and because the secondary minima occurred out of 0.5 phase (including the duration of the eclipse times which are different from each other) we can say that the eccentricity of the system must be larger than zero.

Since the light elements given with equation (1) by Prša et al. (2022) were derived using only Sector 19 data, we primarily obtained a full set of minima times from the current observations. Using the *TESS* observations, we obtained 8 primary and 7 secondary eclipse times. The eclipse times were calculated by using the Minima27[7] software published by Dr. Bob Nelson. In Table 2 we present the calculated minima times with their errors. Additionally, we include the minima times found in the literature. The minima times published in HJD were converted to BJD using the algorithm published by Eastman et al. (2010)[8].

The time span of the primary and secondary minima is about 11,433 and 3639 days, respectively. Applying a linear fit to the $(O-C)$ data (see Figure 3) we obtained new light elements as,

$$Min.I(BJD) = 2458825.167737(0.00109) + 7.06625839(0.00000202) \times E\,, \quad (2)$$

$$Min.II(BJD) = 2458822.747588(0.00214) + 7.06622709(0.00001452) \times E\,. \quad (3)$$

[7] https://www.variablestarssouth.org/resources/bob-nelsons-softwaretools/softwareby-bob-nelson.

[8] https://astroutils.astronomy.osu.edu/time/hjd2bjd.html.

The difference in orbital periods calculated for the primary and secondary minima is about 1.079 sec which is smaller than the obtained errors. Probably this difference occurred because of the different time span of the times of minima used in the fit. The ratio of the slopes obtained for the fit is ≈0.875. Because of this, the $(O-C)$ values between the primary and secondary minima is going to be larger at larger Epoch values. We think that there are not enough data or time span to draw a firm conclusion about apsidal motion as mentioned by Zasche et al. (2018). For the rest of the calculation, we used the light elements obtained for the primary minima.

3. LIGHT CURVE ANALYSIS

Because of the calculation time we obtained a total of 1000 points by averaging at 0.001 phase intervals. By using these phase intervals, we see that the depth of both minima was not changed. For the light curve analysis, we prefer to use the Wilson-Devinney code (2015 version which in 2019 added the *TESS* band to the code) which can solve light curves in magnitudes or in flux. The subscripts 1 and 2 refer to the primary (hotter) and the secondary (cooler) component, respectively.

Before light curve analysis we can find the eccentricity and argument of periastron of the orbit by using the widths of the primary (w_1) and secondary (w_2) eclipses and the phase of the secondary eclipse (φ_2).

$$e_0 \cos w_0 = \frac{\pi}{2}\left[(\varphi_2 - \varphi_1) - 0.5\right] = 0.1241\,, \quad (4)$$

$$e_0 \sin w_0 = \frac{w_2 - w_1}{w_2 + w_1} = 0.1136\,. \quad (5)$$

The required data are given as 0.039, 0.049, and 0.579, respectively by Prša et al. (2022). Using the formulae given by Kopal (1978) (equations 4 and 5) and the phase of the primary eclipse as $\varphi_1 = 0$ we obtained the eccentricity and argument of periastron as 0.1683 and 42.48 deg, respectively. These are used as input parameters in the light curve analysis of the eclipsing system.

In Table 3 we compiled effective temperatures published in different sources (except the last one which was obtained according to the $\log T_{\rm eff} - (B-V)_0$ relation given by Eker et al. 2020) but using the $(B-V) = 0.20$ color and $E(B-V) = 0.087$ reddening values given by Kervella et al. (2019). The median and average of the effective temperatures are found to be 8006 ± 329 K and 8200 ± 329 K, respectively, and we prefer to use these values for the primary component in the light curve analysis of DT Cam.

TABLE 2

THE OBTAINED ECLIPSE TIMES AND ERRORS OF DT CAM

No	Min.Type	HJD (2400000+)	BJD (2400000+)	$\pm\sigma$	References
1	I	48501.35500	48501.35568	-	Otero et al. (2005)
2	I	48543.75800	48543.75868	0.03	Kim et al. (2018)
3	I	51476.27300	51476.27373	0.02	Kim et al. (2018)
4	I	55977.46852	55977.46928	0.00011	Zasche et al. (2014)
5	I	55984.52776	55984.52852	0.00292	Zasche et al. (2018)
6	I	56203.58753	56203.58830	0.00016	Zasche et al. (2014)
7	I	56281.31626	56281.31703	0.00019	Zasche et al. (2017)
8	II	56292.47172	56292.47249	0.00058	Zasche et al. (2017)
9	I	57263.52491	57263.52570	0.0001	Juryšek et al. (2017)
10	I	57355.38700	57355.38780	0.01	Paschke (2017)
11	II	57691.58808	57691.58889	0.00066	Zasche et al. (2017)
12	I	57842.95506	57842.95588	0.00302	Zasche et al. (2018)
13	II	57847.03660	57847.03742	0.0103	Zasche et al. (2018)
14	II	58080.22056	58080.22139	0.0063	Zasche et al. (2018)
15	I	58535.44700	58535.44784	0.0020	Paschke (2019)
16	I	58832.23170	58832.23253	-	Jeong et al. (2020)
17	I	-	58818.10004	0.00001	*TESS*
18	II	-	58822.19000	0.00003	*TESS*
19	I	-	58825.16628	0.00001	*TESS*
20	II	-	58829.25608	0.00003	*TESS*
21	I	-	58832.23254	0.00001	*TESS*
22	II	-	58836.32227	0.00004	*TESS*
23	I	-	58839.29886	0.00001	*TESS*
24	I	59164.34600	59164.34683	0.005	Paschke (2021)
25	II	59182.59000	59182.59083	0.010	Paschke (2021)
26	II	-	59910.39548	0.00002	*TESS*
27	I	-	59913.37222	0.00001	*TESS*
28	II	-	59917.46170	0.00002	*TESS*
29	I	-	59920.43845	0.00001	*TESS*
30	II	-	59924.52798	0.00002	*TESS*
31	I	-	59927.50474	0.00001	*TESS*
32	II	-	59931.59433	0.00002	*TESS*
33	I	-	59934.57104	0.00001	*TESS*

TABLE 3

DT CAM $T_{\rm EFF}$ VALUES FROM LITERATURE

$T_{\rm eff}$ (K)	References
8970	Wright et al. (2003)
8589	Ammons et al. (2006)
7948	McDonald et al. (2012)
7947	Chandler et al. (2016)
7962	McDonald et al. (2017)
8006	Tonry et al. (2018)
8006	*Gaia* Collaboration (2018)
8200	Stassun et al. (2019)
7987	Bai et al. (2019)
8200	Paegert et al. (2021)
8381	Eker et al. (2020)

In the catalogue of Gaia DR3 Part 3 for non-single stars (*Gaia* Collaboration 2022) we found the system's center of mass velocity as $V_\gamma = 13.111 \pm 0.170$ km/s, the semi-amplitude of the primary and secondary component as $K_1 = 73.246 \pm 0.406$ km/s and $K_2 = 92.856 \pm 0.400$ km/s, respectively. Additionally, the system's eccentricity, $e = 0.160 \pm 0.003$, and the argument of periastron, $\omega = 39.123 \pm 1.285$ deg, were obtained, which are compatible with the calculated data by using equations (4) and (5). According to the values given in Gaia DR3 catalogue the mass ratio of the system is obtained as $q(m_2/m_1) = 0.7888$.

The Wilson & Devinney method (Wilson & Devinney 1971; Wilson 1979, 1990) was applied to solve the light curve of the DT Cam. In the light curve analysis of the DT Cam, we used Mode 2 appropriate for detached type systems. Ad-

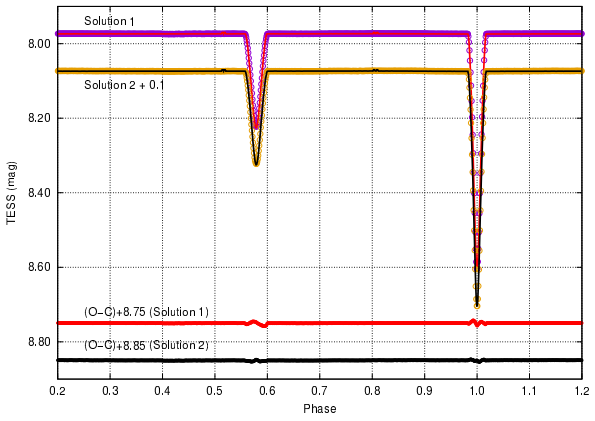

Fig. 4. The observational and theoretical light curves of DT Cam including the residuals of the fit for both solutions. The color figure can be viewed online.

ditionally, we selected the starting parameters as $T_{\rm eff,1} = 8006\,{\rm K}$ (Solution 1) and 8200 K (Solution 2), $e = 0.168$, $\omega = 42.48$ deg, $P = 7.06626244$ days. Because $T_{\rm eff,1}$ is higher than 7200 K, we used the primary's albedo and gravity darkening parameters as 1.0. Assuming the secondary temperature is lower than the primary's we selected $T_{\rm eff,2} = 6500\,{\rm K}$, and included albedo and gravity darkening parameters as 0.5 and 0.32, respectively.

By using the initial parameters (T_1, q, i, e, ω) as input values we solved the light curves until the solution converged. After a coarse solution was obtained, we let the l_3 (third-light) parameter free because of the system is located in a crowded region. The convergent solution was obtained with the adjustable parameters by iteration, until the correction of the parameters became smaller than the corresponding standard deviations. The observed and theoretical light curves, calculated with the final elements, are shown in Figure 4 including the residuals of the fit with the observations.

The parameters obtained from the light curve analysis are given in Table 4. The absolute parameters of the components obtained by the Wilson-Devinney LC code for the DT Cam system are given in Table 5. Since the LC code does not give the errors of the absolute parameters, we estimated them from the input parameters. The errors given here correspond to the propagated errors of the calculated parameters.

Using the bolometric magnitude and bolometric correction for the primary component as 2.694 ± 0.178 and 0.022, respectively, we obtained the absolute magnitude of the primary component as $M_{V,1} = 2.672 \pm 0.279$. In the ASAS-SN Catalogue of Variable Stars II database[9] the mean V magnitude of the system is given as $8^m.63$ and it is nearly 0.5 magnitudes dimmer than the given value in the Simbad database. The $(B-V)$ and $E(B-V)$ values given in the ASAS-SN Catalogue as 0.093 and 0.577, respectively, are different from the values found in the literature. By using $(B-V) = 0.2$ and $E(B-V) = 0.07$ we obtained the interstellar extinction in the V filter as $A_v = 3.1 \times E(B-V) = 0.317$. Using those values, we obtained the distance of the DT Cam as 174 ± 10 pc, which is consistent with that given in the *TESS* Input Catalogue (Stassun et al. 2019) and in Gaia DR3 catalogues as 183.927 and 183.479 pc, respectively.

4. OUT-OF-ECLIPSE LIGHT VARIATION

Due to the relatively large amplitude of the eclipse variation, we cannot visually see any light variations at the maxima of the light curve. In Figure 4, we see that the light at the maxima is fairly smooth. Since the primary component's temperature is located in the instability strip, we suspect that it could be a pulsator, similar to stars δ Scuti or γ Dor. In Figure 5 we plot the out-of-eclipse variation for Sectors 19 (upper panel) and 59 (lower panel) included the eclipse boundaries with the regions of ingress and egress to the eclipse indicated by horizontal error bars. As can be seen in Figure 5 despite scattering (gray dots) there are multi periodic variations which can be attributed to pulsation or any other type of variation, like rotation. Because of scattering, we prefer to smooth the light curves by obtaining an average of 5 successive observations (black dots in Figure 5).

The time gap between Sector 19 and 59 is approximately 1069 days. Because of this we prefer to analyze the data separately in the frequency domain. The obtained frequencies are given in Table 6, and the amplitude variation in Figure 6 includes the Fourier fit in Figure 7. The Rayleigh resolution for Sectors 19 and 59 were obtained as $0.040 d^{-1}$ and $0.038 d^{-1}$, respectively. All of the marked combinations given in Table 6 are obtained as the difference between the observed and the predicted frequencies which are smaller than or equal to the Rayleigh criterion.

The existence of periodic variations can be clearly seen by using the normal points created. We found that most of the frequencies obtained are related to the orbital period, except the frequency obtained at $1.65 d^{-1}$, which corresponds to 0.605 days. The

[9] https://asas-sn.osu.edu/variables/531066b2-10c7-52cb-8856-d6a54c9843ee.

TABLE 4

THE LIGHT CURVE SOLUTION OF DT CAM

	Solution 1		Solution 2	
Parameters	**Value**	$\pm\sigma$	**Value**	$\pm\sigma$
T_0(BJD)	2458825.16774	0.00109	-	-
P (day)	7.06625839	0.000002	-	-
a($R_\odot$)	22.859	0.024	-	-
V_γ(km/s)	13.111	0.170	-	-
K_1(km/s)	73.246	0.406	-	-
K_2(km/s)	92.856	0.400	-	-
e	0.167	0.001	0.164	0.002
ω(deg)	42.643	0.029	41.060	0.059
$q(m_2/m_1)$	0.7888	-	-	-
Phase Shift	0.0360	-	0.0360	-
i(deg)	87.675	0.006	88.194	0.010
T_1(K)	8006*	329*	8200*	329*
T_2(K)	6368	250*	6448	250*
A_1	1.000	-	1.000	-
A_2	0.500	-	0.500	-
g_1	1.000	-	1.000	-
g_2	0.320	-	0.320	-
Ω_1	17.82053	0.00665	18.10684	0.01549
Ω_2	13.15815	0.00381	13.08262	0.00824
x_1 (bolo)	0.651	-	-	-
x_2 (bolo)	0.640	-	-	-
y_1 (bolo)	0.255	-	-	-
y_2 (bolo)	0.234	-	-	-
L_1/L_{tot}(TESS)	0.60057	0.00078	0.59815	0.00148
$L_3/L_{tot}(TESS)$	0.00920	-	0.01639	-
$r1$(mean)	0.05928	0.00002	0.05827	0.00003
$r2$(mean)	0.06658	0.00002	0.06697	0.00003
σ(fit)	-	2.6245E-07	-	5.3357E-07

Assumed values are marked with asterisks.

strongest amplitude (essentially semi-amplitude) is of the order of 0.0003 mag in the *TESS* filter. The amplitude in Johnson V is not known but we can estimate it using the relation given by Paunzen et al. (2020) as $Amp(V)/Amp(TESS) = 1.44(4)$. According to this relation, the estimated amplitude in Johnson V is about 0.00086 mag and we cannot obtain such a low magnitude variation with ordinary photometric Earth bound observations. As can be seen in Figure 6, the real amplitude of the periodic variation is probably larger than that obtained by Fourier analysis.

Grigahcène et al. (2010) characterized the δ Scuti type variables as short period pulsating stars, with periods between 0.014 (f = 71.428 d^{-1}) and 0.333 (f = 3.003 d^{-1}) days and pulsation constant Q (Handler et al. 2002) lower than 0.055 days, but generally the accepted lower limit is smaller than 0.033 days (Stellingwerf 1979; Breger 1990).

The binary model yields a mean density of $\rho_1 = 0.721\rho_\odot$ and $\rho_2 = 0.401\rho_\odot$ for the primary and secondary component, respectively. The frequency for the highest amplitude variations for Sector 19 found to be $f_1 = 1.650234d^{-1}$ ($P_1 = 0.60597$ days). Using the relation given as $Q = P_{puls}\sqrt{(\rho/\rho_\odot)}$, we obtained the pulsation constant as $Q_1 = 0.514$ and $Q_2 = 0.384$ days for the primary and secondary component, respectively. As can be seen all of the pulsation constants are larger than 0.055 days. According to these results (including the period of the cyclic variation) we conclude that none of the components can be a δ Scuti pulsator.

TABLE 5

ABSOLUTE PARAMETERS OF DT CAM

	Solution 1		Solution 2	
Parameters	Primary	Secondary	Primary	Secondary
Mass ($M_\odot$)	1.793 ± 0.007	1.414 ± 0.006	1.793 ± 0.007	1.414 ± 0.006
Radius ($R_\odot$)	1.340 ± 0.002	1.538 ± 0.002	1.332 ± 0.002	1.531 ± 0.002
Luminosity* ($L_\odot$)	6.796 ± 1.117	3.432 ± 0.539	7.227 ± 1.160	3.651 ± 0.566
$\rho(\rho_\odot)$	0.721	0.401	0.759	0.394
M_{bol}	2.669 ± 0.178	3.411 ± 0.171	2.603 ± 0.174	3.344 ± 0.168
Bol.Corr.(BC)	0.022	0.062	0.003	0.068
M_v	2.647 ± 0.279	3.349 ± 0.274	2.600 ± 0.277	3.276 ± 0.273
log g (cgs)	4.428 ± 0.002	4.224 ± 0.002	4.443 ± 0.002	4.219 ± 0.002
d(pc)	174 ± 10	-	178 ± 10	-

*Calculated by using components' temperature and radius.

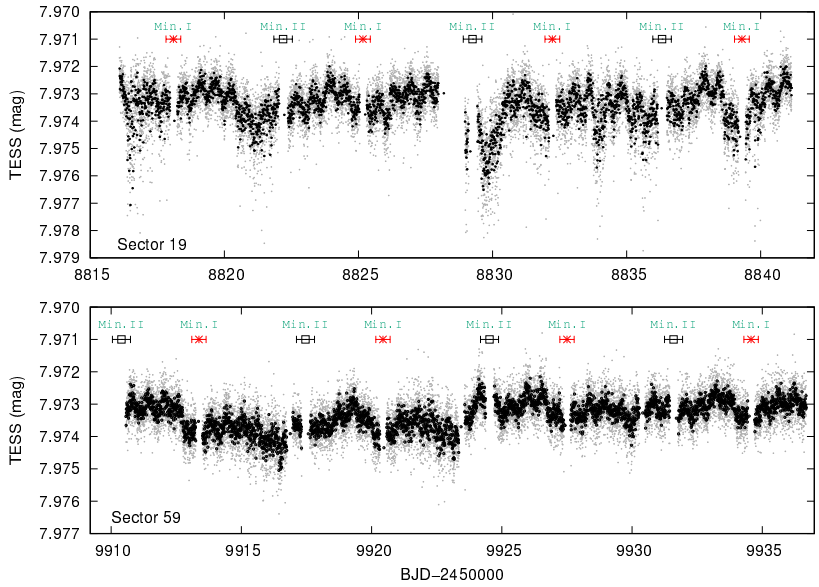

Fig. 5. Out-of-eclipse variation of DT Cam for Sectors 19 (upper panel) and 59 (lower panel). Black dots represent the average of 5 successive observations. The color figure can be viewed online.

The location of the secondary component in the HR diagram coincides with the Solar-like pulsators but the pulsation period is much larger than the 3 to 10 min ranges given by Aerts et al. (2010). Because of this we conclude that the secondary component cannot be a Solar-like pulsator.

Kaye et al. (1999) characterized the γ Doradus (GDOR) type variables as high-order, low-degree, non-radial gravity mode pulsators and showed that the period range is $0.3 \leq P(day) \leq 3 (0.33 \leq f(d^{-1}) \leq 3.33)$. Among the GDOR type pulsators there are low- and high-amplitude examples; the high-amplitude ones are explained by the superposition of several base frequencies (Paunzen et al. 2020). Most of the GDOR pulsators are in the region of A- and F-type main sequence stars within the temperature range of $6100 < T_{\rm eff} < 7500$ K (Bradley et al. 2015). Additionally, Q pulsation constants for GDOR type stars are given as $Q > 0.24$ days (Grigahcène et al. 2010).

All of the parameters obtained for the secondary component; effective temperature ($T_2 = 6368$ K), Q pulsation constant ($Q_2 = 0.384$ days), and frequency of the periodic variation ($f = 1.65 d^{-1}$) show that the secondary component can be a GDOR type pulsator. In Figure 8 we see that the secondary component is located out of the instability strip given for GDOR type pulsators. But we also see that a small number

TABLE 6

THE OBTAINED SIGNIFICANT FREQUENCIES OF DT CAM USING OUT-OF-ECLIPSE DATA FOR SECTORS 19 AND 59

No	Frequency (d^{-1})	Amplitude *TESS* (mag)	Phase (rad)	P(days)	P_{orb}/P	n	Difference	Combination
			Sector 19					
f_1	1.650234	0.000324	0.119240	0.60597	11.661	-	-	-
f_2	0.227481	0.000198	0.613891	4.39598	1.607	-	-	-
f_3	0.431016	0.000162	0.622711	2.32010	3.046	3	-0.0065	$3f_{orb}$
f_4	0.277367	0.000325	0.363430	3.60533	1.960	2	0.0057	$2f_{orb}$
f_5	0.133695	0.000213	0.403955	7.47972	0.945	1	0.0078	f_{orb}
f_6	0.319271	0.000168	0.512517	3.13213	2.256	-	-	-
f_7	0.041904	0.000141	0.513211	23.86387	0.296	-	-	-
			Sector 59					
f_1	0.034459	0.000330	0.634004	29.02023	0.243	0.25	0.0009	$f_{orb}/4$
f_2	1.652104	0.000180	0.165151	0.60529	11.674	-	-	-
f_3	0.141664	0.000170	0.828329	7.05898	1.001	1	-0.0001	f_{orb}
f_4	0.428820	0.000206	0.133727	2.33198	3.030	3	-0.0043	$3f_{orb}$
f_5	0.070832	0.000153	0.887096	14.11795	0.501	0.5	-0.0001	$f_{orb}/2$
f_6	0.277584	0.000103	0.481096	3.60251	1.961	2	0.0055	$2f_{orb}$
f_7	0.111034	0.000097	0.965751	9.00628	0.785	-	0.0038	$f_3 - f_1$ (f_{orb}-$f_{orb}/4$)

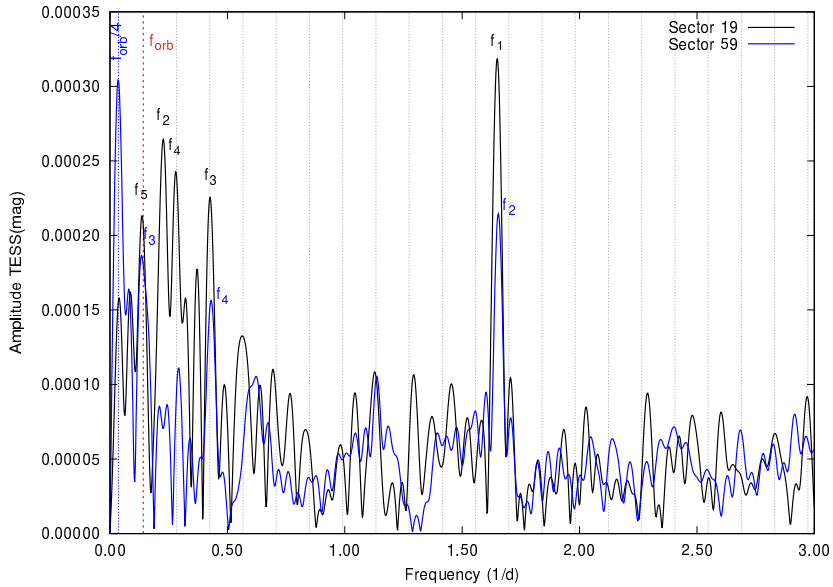

Fig. 6. The amplitude spectrum for the out-of-eclipse light variation of DT Cam for Sectors 19 (black line) and 59 (blue line). We marked the location of the orbital frequency (red vertical line) including the harmonics of orbital frequency f_{orb} with dotted vertical lines. The color figure can be viewed online.

of GDORs are located outside this instability strip too, which can be a sign of the type of the pulsator.

By using Kepler observations, Balona (2011) showed that low-frequency variations are present in most A-type stars and that the dominant period is consistent with the expected rotational periods of these stars. Using this finding Balona (2011) suggested that star spots, or other co-rotating structures, may be responsible for the low-amplitude light variations in normal A-type stars. Comparison of the two sectors with each other in Figure 6 (the amplitude of frequency at 1.65 d^{-1}) we see that the am-

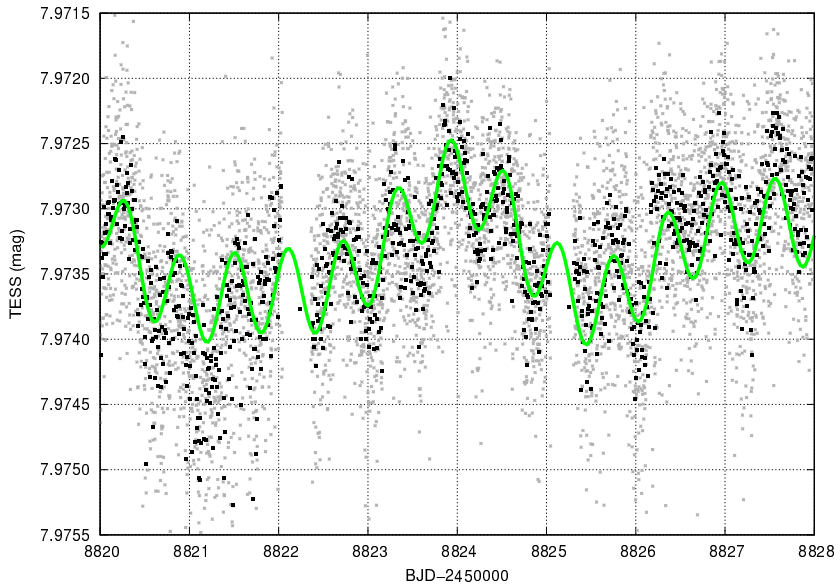

Fig. 7. Small amplitude periodic variation of DT Cam at Sector 19 (a small portion is plotted). The synthetic curve was computed using all the frequencies detected. Gray dots are for the original data, black dots represent the average of 5 successive observations, and the green line is the Fourier fit obtained by using all of the frequencies given in Table 6 for Sector 19. The color figure can be viewed online.

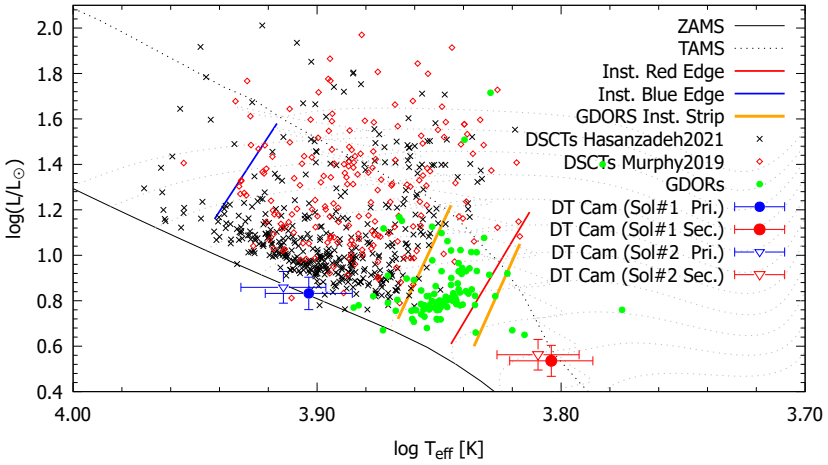

Fig. 8. Position of the primary and secondary component of DT Cam in the Hertzsprung-Russell diagram (HRD) (blue and red points, respectively). Black and gray continuous lines show the ZAMS and evolutionary tracks of stars for solar metallicity composition Z=0.008, taken from Girardi et al. (2000). Dotted red and blue lines represent the boundaries of the instability strip. Dashed orange lines indicate the theoretical cool and hot boundary of the γ Doradus instability strip (Warner et al. 2003). The other small dots represent the location of δ Scuti type stars obtained from Hasanzadeh et al. (2021) (black) and Murphy et al. (2019) (red). Green dots show confirmed γ Doradus stars compiled from Kaye et al. (1999), Henry et al. (2005), and Paunzen et al. (2020). The color figure can be viewed online.

plitude is essentially different in both sectors, which can be a sign of variable amplitude. And this can be a sign of stars pots as mentioned by Lanza et al. (2009) for cool stars. Because of this, there is a possibility of the secondary component, the cooler component, having star spots on the surface. Balona (2011) showed that there is a possibility of the A-type component also having star spots on its surface, and found that a total of 208 A-type stars which are coded as SPOT in their work show only a single peak

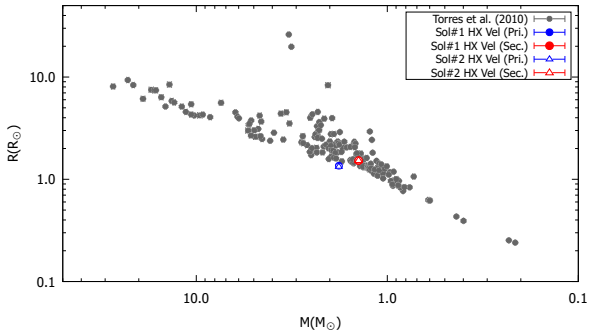

Fig. 9. Position of the primary and secondary component of DT Cam on the mass-radius diagram (blue and red points, respectively). The mass and radius values were taken from Torres et al. (2010). The color figure can be viewed online.

in the frequency domain, as we obtained for the DT Cam system

Assuming that the frequency of highest amplitude is the rotation frequency we can calculate the rotational velocity of the components separately by using the radius values given in Table 5. The rotational velocities obtained for the primary and secondary components are $v_1 = 112.57$ km/s and $v_2 = 129.20$ km/s, respectively. In the literature we found that the average rotational velocities of A0 and F5 type main-sequence stars were given as 190 and 25 km/s, respectively (McNally 1965). Using the corresponding spectral types for the components as A2+F4 we concluded that the low amplitude periodic variation with a period of 0.60597 days can be caused by the rotation of the primary component. In the literature e.g. Sikora et al. (2019) we find some examples, such as HD 13709, HD 19398, and HD 54558, for which the rotational period is smaller than that obtained for the A2-type primary component in DT Cam system.

5. RESULTS AND DISCUSSION

We derived for the first time the absolute and geometrical parameters of the Algol type eccentric eclipsing binary DT Cam by using *TESS* and Gaia observations.The results of the light-curve modelling reveal that DT Cam is a detached system with one of the components probably in the PMS phase. Using the semi-amplitudes of the radial velocity data of the system given in the catalogues, combined with our light curve solution, enabled us to find the physical and geometric parameters of the components. In this sense, we conclude that the system will provide an important contribution to the literature.

We updated the light elements of the system by using all of the times of minima obtained by the *TESS* observations and data found in the literature. The difference of the orbital period obtained for the primary and secondary minima is 1.079 seconds, and it is probably caused by the different time spans of the observations. In addition, we think that there is not enough time span for obtaining apsidal motion parameters.

In Figure 8 we plot our results with the δ Scuti type variables compiled from Uytterhoeven et al. (2011) and Murphy et al. (2019) including the γ Doradus pulsators compiled from Kaye et al. (1999), Henry et al. (2005), and Paunzen et al. (2020). The primary component is located on the Main Sequence of the instability strip. Because of the location of the components on the HRD we suspected that the primary or secondary component can be a pulsator like δ Scuti or γ Doradus, or a rotational variable. Based on the physical and frequency analysis parameters discussed in the previous section we cannot strictly figure out which of the components shows a small amplitude periodic variation. As a result, the secondary component can be a GDOR type pulsator or the A2-type component can be a rotating variable. Because most of GDOR type pulsators show multi-period variations (Zhou 2015; Paunzen et al. 2020; Takata et al. 2020; Henry et al. 2005) and since we see only one for DT Cam, we accepted that the primary component is a rotating variable.

The number of eclipsing binaries with a pre-main sequence component whose absolute parameters are determined is very small. In this sense we think that the system will make an important contribution for the understanding of stellar structure and evolution.

In Figure 9 we plot our results in the mass-radius diagram given by Torres et al. (2010). The primary component seems to have a small radius and low luminosity. Most likely, the primary component has a very fast rotating core, as in the EK Cep system investigated by Yıldız (2003).

As obtained in § 4 the out-of-eclipse variations are mostly related to the orbital frequency, except for the low amplitude periodic variation with a period of 0.60597 days. It is not possible to say whether these small-amplitude periodic variations are caused by one or both components. If the periodic variation of 0.60597 days is caused by rotation of the primary component we can say that system is not synchronized.

We thank the anonymous referee for helpful comments and suggestions that greatly improved

the quality of this paper, especially because of the warning that the secondary component may be a pre-main sequence object. This research has made use of VizieR the Simbad database, operated at CDS, Strasbourg, France, and NASA's Astrophysics Data System Abstract Service. This work has made use of data from the European Space Agency (ESA) mission Gaia (https://www.cosmos.esa.int/gaia), processed by the Gaia Data Processing and Analysis Consortium (DPAC7). Funding for the DPAC has been provided by national institutions, in particular the institutions participating in the Gaia Multilateral Agreement. The *TESS* data presented in this paper were obtained from the Mikulski Archive for Space Telescopes (MAST). Funding for the *TESS* mission is provided by the NASA Explorer Program.

REFERENCES

Aerts, C., Christensen-Dalsgaard, J., Kurtz, D. W. 2010, Asteroseismology (Springer), https://doi.org/10.1007/978-1-4020-5803-5

Ammons, S. M., Robinson, S. E., Strader J., et al. 2006, ApJ, 638, 1004, https://doi.org/10.1086/498490

Avvakumova, E. A., Malkov, O. Y., & Kniazev, A. Y. 2013, AN, 334, 860, https://doi.org/10.1002/asna.201311942

Bai, Y., Liu, J. F., Bai, Z. R., Wang, S., & Fan, D. W. 2019, AJ, 158, 93, https://doi.org/10.3847/1538-3881/ab3048

Balona, L. A. 2011, MNRAS, 415, 1691, https://doi.org/10.1111/j.1365-2966.2011.18813.x

Bradley, P. A., Guzik, J. A., Miles, L. F., et al. 2015, AJ, 149, 68, https://doi.org/10.1088/0004-6256/149/2/68

Breger, M. 1990, Delta Scuti Star, ed. M. Breger and Michael Montgomery (San Francisco, CA: ASPC)

Burggraaff, O., Talens, G. J. J., Spronck, J., et al. 2018, A&A, 617, 32, https://doi.org/10.1051/0004-6361/201833142

Cannon, A. J. & Pickering, E. C. 1993, yCat, 3135, 0

Chandler, C. O., McDonald, I., & Kane, S. R. 2016, AJ, 151, 59, https://doi.org/10.3847/0004-6256/151/3/59

Eastman, J., Siverd, R., & Gaudi, B. S. 2010, PASP, 122, 935, https://doi.org/10.1086/655938

Eker, Z., Soydugan, F., Bilir, S., et al. 2020, MNRAS, 496, 3887, https://doi.org/10.1093/mnras/staa1659

Gaia Collaboration. 2018, 2018yCat.1345, 0G, https://doi.org/10.26093/cds/vizier.1345

Gaia Collaboration. 2022, 2022yCat.1355, 0G, https://doi.org/10.26093/cds/vizier.1355

Girardi, L., Bressan, A., Bertelli, G., & Chiosi, C. 2000, A&AS, 141, 371, https://doi.org/10.1051/aas:2000126

Grigahcène, A., Antoci, V., Balona, L., et al. 2010, ApJ, 713, 192, https://doi.org/10.1088/2041-8205/713/2/L192

Handler, G. & Shobbrook, R. R. 2002, MNRAS, 333, 251, https://doi.org/10.1046/j.1365-8711.2002.05401.x

Hasanzadeh, A., Safari, H., & Ghasemi, H. 2021, MNRAS, 505, 1476, https://doi.org/10.1093/mnras/stab1411

Henry, G. W., Fekel, F. C., & Henry S. M. 2005, AJ, 129, 2815, https://doi.org/10.1086/429876

Henry, G. W., Fekel, F. C., & Williamson M. H. 2022, AJ, 163, 180, https://doi.org/10.3847/1538-3881/ac540b

Jeong, M. -J., Kim, C. -H., Song, M. -H., et al. 2020, OEJV, 205, https://doi.org/0.5817/OEJV2020-0205

Juryšek, J., Hoňková, K., Šmelcer, L., et al. 2017, EIJV, 179, 1

Kaye, A. B., Handler, G., Krisciunas, K., et al. 1999, PASP, 111, 840, https://doi.org/10.1086/316399

Kervella, P., Arenou, F., Mignard, F., & Thévenin, F. 2019, A&A, 623, 72, https://doi.org/10.1051/0004-6361/201834371

Kervella, P., Arenou, F., & Thévenin, F. 2022, A&A, 657, 7, https://doi.org/10.1051/0004-6361/202142146

Kim, C. -H., Kreiner, J. M., Zakrzewski, B., et al. 2018, ApJS, 235, 41, https://doi.org/10.3847/1538-4365/aab7ef

Kopal, Z. 1978, ASSL, 68, https://doi.org/10.1007/978-94-009-9780-6

Lanza, A. F., Pagano, I., Leto, G., et al. 2009, A&A, 493, 193, https://doi.org/10.1051/0004-6361:200810591

McDonald, I., Zijlstra, A. A., & Boyer M. L. 2012, MNRAS, 427, 343, https://doi.org/10.1111/j.1365-2966.2012.21873.x

McDonald, I., Zijlstra, A. A., & Watson, R. A. 2017, MNRAS, 471, 770, https://doi.org/10.1093/mnras/stx1433

McNally, D. 1965, The Observatory, 85, 166

Murphy, S. J., Hey, D., Van Reeth, T., & Bedding T. R. 2019, MNRAS, 485, 2380, https://doi.org/10.1093/mnras/stz590

Otero, S. A., Wils, P., & Dubovsky, P. A. 2005, IBVS, 5586, 1

Paegert, M., Stassun, K. G., Collins, K. A., et al. 2021, arXiv:2108.04778, https://doi.org/10.48550/arXiv.2108.04778

Paschke, A. 2017, OEJV, 181

_____. 2019, BAVJ, 30, 1

_____. 2021, BAVJ, 55, 1

Paunzen, E., Bernhard, K., Hümmerich, S., et al. 2020, MNRAS, 499, 3976, https://doi.org/10.1093/mnras/staa2905

Prša, A., Kochoska, A., Conroy, K. E. et al. 2022, ApJS, 258, 16, https://doi.org/10.3847/1538-4365/ac324a

Ricker, G. R., Winn, J. N., Vanderspek, R., et al. 2015, JATIS, 1. 014003, https://doi.org/10.1117/1.JATIS.1.1.014003

Shi, Xiang-dong, Sheng-bang, Qian, & Lin-Jia Li. 2022, ApJS, 259, 50, https://doi.org/10.3847/1538-4365/ac59b9

Sikora, J., David-Uraz, A., Chowdhury, S., et al. 2019, MNRAS, 487, 4695, https://doi.org/10.193/mnars/stz1581

Stassun, K. G., Oelkers, R. J., Paegert, M., et al. 2019, AJ, 158, 138, https://doi.org/10.3847/1538-3881/ab3467

Stellingwerf, R. F. 1979, ApJ, 227, 935, https://doi.org/10.1086/156802

Takata, M., Ouzzani, R.-M., Saio, H., et al. 2020, A&A, 635, 106, https://doi.org/10.1051/0004-6361/201936297

Tonry, J. L., Denneau, L., Flewelling, H., et al. 2018, ApJ, 867, 105, https://doi.org/10.3847/1538-4357/aae386

Torres, G., Andersen, J., & Giménez, A. 2010, A&ARv, 18, 67, https://doi.org/10.1007/s00159-009-0025-1

Uytterhoeven, K., Moya, A., Grigahcène, A., et al. 2011, A&A, 534, 125, https://doi.org/10.1051/0004-6361/201117368

Warner P. B., Kaye A. B., & Guzik, J. A. 2003, ApJ, 593, 1049, https://doi.org/10.1086/376727

Wilson, R. E. & Devinney, E. J. 1971, ApJ, 166, 605, https://doi.org/10.1086/150986

Wilson, R. E. 1979, ApJ, 234, 1054, https://doi.org/10.1086/157588

———. 1990, ApJ, 256, 613, https://doi.org/10.1086/168867

Wright, C. O., Egan, M. P., Kraemer, K. E., & Price, S. D. 2003, AJ, 125, 359, https://doi.org/10.1086/345511

Yıldız, M. 2003, A&A, 409, 689, https://doi.org/10.1051/0004-6361:20031118

Zasche, P., Uhlar, R., Kucakova, H., Svoboda, P., & Masek, M. 2014, IBVS, 6114, 1

Zasche, P., Uhlar, R., Svoboda, P., et al. 2017, IBVS 6204, https://doi.org/10.22444/IBVS.6204

Zasche, P., Wolf, M., Uhlar, R., et al. 2018, A&A, 619, 85, https://doi.org/10.1051/0004-6361/201832793

Zhou, A. Y. 2015, arXiv:1501.05166, https://doi.org/10.48550/arXiv.1501.05166

B. Gürol: Ankara University, Science Faculty, Dept. of Astronomy and Space Sciences, 06100 Tandoğan, Ankara, Turkey (Birol.Gurol@ankara.edu.tr).

T. Özdemir: İnonu University, Faculty of Arts and Sciences, Malatya, Turkey (tuncay@inonu.edu.tr).